

UCSF

UC San Francisco Previously Published Works

Title

NHE1 Regulates the Stratum Corneum Permeability Barrier Homeostasis
MICROENVIRONMENT ACIDIFICATION ASSESSED WITH FLUORESCENCE LIFETIME IMAGING*

Permalink

<https://escholarship.org/uc/item/1773k9t5>

Journal

Journal of Biological Chemistry, 277(49)

ISSN

0021-9258

Authors

Behne, Martin J
Meyer, Jamie W
Hanson, Kerry M
[et al.](#)

Publication Date

2002-12-01

DOI

10.1074/jbc.m204759200

Copyright Information

This work is made available under the terms of a Creative Commons Attribution License, available at <https://creativecommons.org/licenses/by/4.0/>

Peer reviewed

NHE1 Regulates the Stratum Corneum Permeability Barrier Homeostasis

MICROENVIRONMENT ACIDIFICATION ASSESSED WITH FLUORESCENCE LIFETIME IMAGING*

Received for publication, May 15, 2002, and in revised form, September 4, 2002
Published, JBC Papers in Press, September 7, 2002, DOI 10.1074/jbc.M204759200

Martin J. Behne^{‡§}, Jamie W. Meyer[¶], Kerry M. Hanson^{**}, Nicholas P. Barry^{**}, Satoru Murata[‡], Debra Crumrine[‡], Robert W. Clegg^{**}, Enrico Gratton^{**}, Walter M. Holleran[‡], Peter M. Elias[‡], and Theodora M. Mauro[‡]

From the [‡]Dermatology Service, Veterans Affairs Medical Center and Department of Dermatology, University of California, San Francisco, California 94121, the [¶]Department of Molecular Genetics, Biochemistry, and Microbiology, University of Cincinnati College of Medicine, University of Cincinnati, Cincinnati, Ohio 45267, and the ^{**}Laboratory for Fluorescence Dynamics, Department of Physics, University of Illinois, Urbana-Champaign, Illinois 61801

The outermost epidermal layer, the stratum corneum (SC), exhibits an acidic surface pH, whereas the pH at its base approaches neutrality. NHE1 is the only Na⁺/H⁺ antiporter isoform in keratinocytes and epidermis, and has been shown to regulate intracellular pH. We now demonstrate a novel function for NHE1, as we find that it also controls acidification of extracellular “microdomains” in the SC that are essential for activation of pH-sensitive enzymes and the formation of the epidermal permeability barrier. NHE1 expression in epidermis is most pronounced in granular cell layers, and although the surface pH of NHE1 knockout mice is only slightly more alkaline than normal using conventional pH measurements, a more sensitive method, fluorescence lifetime imaging, demonstrates that the acidic intercellular domains at the surface and of the lower SC disappear in NHE1 ^{-/-} animals. Fluorescence lifetime imaging studies also reveal that SC acidification does not occur through a uniform gradient, but through the progressive accumulation of acidic microdomains. These findings not only visualize the spatial distribution of the SC pH gradient, but also demonstrate a role for NHE1 in the generation of acidic extracellular domains of the lower SC, thus providing the acidification of deep SC interstices necessary for lipid processing and barrier homeostasis.

Cultured keratinocytes express the sodium-proton exchanger (NHE)¹ class of non-energy-dependent transporters, which controls intracellular pH (1). Recently, the NHE1 iso-

form has been shown to be the only isoform in keratinocytes and epidermis (2).

Acidification is essential for the epidermal permeability barrier, as shown by the observation that barrier recovery proceeds normally at an acidic pH, but is delayed at a neutral pH (*i.e.* pH 7–7.4) as a result of impaired post-secretory processing of secreted, extracellular lipids in the lower SC (3). The delay in recovery at a neutral pH is explained by the *in situ* activity profiles of β -glucocerebrosidase (β -Glc-Cer'ase), and acid-sphingomyelinase (aSM'ase) in the SC, which lack activity at a neutral pH (4, 5). β -Glc-Cer'ase and aSM'ase comprise two key lipid hydrolases, which are critical for the formation of mature extracellular lamellar bilayers (6, 7), and both are required for the normal processing of secreted polar lipid precursors into their more non-polar species.

The acidic pH of the SC has been attributed largely to mechanisms extrinsic to the epidermis, such as: (a) byproducts of microbial metabolism (8); (b) lactic acid and lactate from sweat (9); (c) free fatty acids (10); (d) progressive desiccation of the SC (11), and/or (e) generation of the organic acid, cis-urocanic acid (cUCA) from filaggrin (12). In this report, we demonstrate that NHE1 deletion or pharmacologic inhibition elevates SC pH and impedes both lipid processing and resulting barrier repair, suggesting this agent is essential in establishing and/or maintaining SC pH.

The aim of this study was to assess the effect of NHE1 on extracellular acidification of the SC and to visualize the spatial distribution of the SC pH gradient. Because the origin and character of the acidic pH of the SC have been difficult to study, we adapted a more sophisticated method, fluorescence lifetime imaging (FLIM), to investigate SC pH (13). Using this method, we find that the pH “gradient” is not uniform, and that NHE1 preferentially acidifies extracellular domains at and just above the stratum granulosum (SG)-SC junction. Moreover, NHE1 expression increases in the outer epidermis, in an increasingly apical pattern, thus providing the acidic milieu necessary for formation of mature extracellular lipid bilayers in the SC.

EXPERIMENTAL PROCEDURES

Materials—Amiloride and HEPES were purchased from Sigma. 2',7'-Bis(carboxyethyl)-5,6-carboxyfluorescein (BCECF) was from Molecular Probes (Eugene, OR). HOE694 was kindly provided by Dr. H. J. Lang (Aventis Pharma Deutschland GmbH, Frankfurt am Main, Germany). All other reagents were of analytical grade.

Animals—Male hairless mice (SKH1 hr/hr, Charles River Laboratories, Wilmington, MA) were fed Purina mouse diet and water *ad libitum*. Animals were 8–12 weeks old at time of experiments. Heterozygous, NHE1-deficient mice (14) were bred locally from heterozygous

* This work was supported in part by National Institutes of Health Grants AR44341 (to T. M. M.), AR19098 (to P. M. E.), and Department of Veterans Affairs Merit Review MAU 3 “Creation and Maintenance of the Epidermal pH Gradient” (to T. M. M.). The costs of publication of this article were defrayed in part by the payment of page charges. This article must therefore be hereby marked “advertisement” in accordance with 18 U.S.C. Section 1734 solely to indicate this fact.

§ Supported by a grant from Sebapharma, Boppard, Germany. To whom correspondence should be addressed: University of California San Francisco and Department of Veterans Affairs Medical Center, Dermatology Service (190), 4150 Clement St., San Francisco, CA 94121. E-mail: behnemj@itsa.ucsf.edu.

¶ Supported in part by funds from National Institutes of Health Grant HL61974 (to Gary Shull).

¹ The abbreviations used are: NHE, sodium-proton exchanger; β -Glc-Cer'ase, β -glucocerebrosidase; aSM'ase, acid-sphingomyelinase; cUCA, cis-urocanic acid; FLIM, fluorescence lifetime imaging; SC, stratum corneum; SG, stratum granulosum; BCECF, 2',7'-bis(carboxyethyl)-5,6-carboxyfluorescein; FITC, fluorescein isothiocyanate.

founders received from Dr. G. E. Shull (Cincinnati, OH), and each litter was genotyped separately. Mice were maintained on a mixed background of SVJ129 and Black Swiss, and inbred for at least 4 generations. Functional experiments were performed on animals aged 6–10 weeks.

Immunohistochemistry—Fresh biopsies from NHE1 $+/+$ or $-/-$ mice were formaldehyde-fixed, paraffin-embedded, and sectioned (5 μm). For immunolabeling of NHE1, a rabbit polyclonal antibody was used (Chemicon International, Temecula, CA), which was detected via a FITC-labeled, secondary goat anti-rabbit antibody (Cappel, Organon Teknika Corp., Durham, NC). Sections were counterstained with propidium iodide (Sigma), and pictures were taken on a Leica TCS-SP confocal microscope.

Fluorescence Lifetime Imaging Microscopy—pH was determined using the lifetime-sensitive fluorescent pH indicator BCECF (Molecular Probes). We have examined the question of possible vehicle toxicity in previous studies and found that applications of propylene glycol/ethanol (in a 7:3 mix) do not exhibit deleterious effects on either permeability barrier function or on the structure of the SC, and do not alter the kinetics of barrier recovery in acute experiments (see, *e.g.*, Ref. 15). Moreover, following prolonged ethanol exposure (twice daily over 7 days), such effects are limited to superficial layers of the SC, where SC interstices are expanded without disrupting the lamellar lipid domains. Even under these conditions, ethanol neither breaches the corneocyte, nor the barrier-forming, lower two thirds of the SC (16), definitely excluding the nucleated layers of the epidermis (17), with no effects on base line barrier function (18). In these experiments, the solvent was a 7:3 mix of propylene glycol and ethanol, used because it produces better SC penetration. Whereas propylene glycol/ethanol elicits the minor effects described above, ethanol alone would be expected to produce even fewer effects because of rapid surface evaporation. The dye was therefore applied in pure ethanol (58–120 μM BCECF), four times over the course of 1 h, and reapplied only after remaining ethanol had evaporated. A biopsy was taken \sim 15 min following the last dye application, mounted for microscopy, and directly visualized (maximum time delay 1 h). Additionally, we examined the possible influence of cholesterol as a key epidermal lipid, and ethanol as the solvent in our experiments on lifetime measurements. A saturated solution of cholesterol in buffer did not affect lifetimes, when corrected for its index of refraction. Similarly, water/ethanol mixtures with up to 5% ethanol also did not change lifetime, even without a correction for refraction.

Two-photon FLIM (19–21) was used to determine pH. The specific protocols used to determine pH as a function of epidermal depth and cellular location were validated (13). In brief, a Millennia-pumped Tsunami titanium:sapphire laser system (Spectra-Physics) was used as the two-photon excitation source. Two-photon excitation of the sample was achieved by coupling the 820-nm output of the laser through the epifluorescence port of a Zeiss Axiovert microscope. Less than 1 milliwatt was used to excite the sample. The excitation beam was diverted to the sample by a dichroic filter, and the fluorescence was collected using a Hamamatsu (R3996) photomultiplier placed at the bottom port of the microscope. Scanning mirrors and a 40 \times infinity corrected oil objective (Zeiss F Fluor, 1.3 numeric aperture) were used to image areas of 214 μm^2 . Z-slices (1.7 $\mu\text{m}/\text{slice}$) were obtained by adjusting the objective focus with a motorized driver (ASI Multi-Scan 4). Lifetime data were acquired using the frequency-domain method (80 MHz). Fluorescein was used as the reference lifetime standard ($\tau_f = 4.05$ ns, pH 9.5). Data evaluation and visualization were performed directly with the in-house software SIM-FCS. Fluorescence intensity images were adjusted to enhance structural features and to visualize dye distribution and penetration. Lifetime values were converted to pH values, based on a calibration of BCECF in a series of buffers of different pH. The resulting pH maps are displayed on the same color scale to facilitate comparisons. The pH value distribution within these images is depicted in the corresponding histograms. Individual images in Fig. 2 were combined using Adobe Illustrator (Adobe Systems Inc., San Jose, CA), but no further image processing was performed. Background fluorescence was measured in samples of unstained tissue, treated otherwise identically. Intensity counts were always below 10/50 μs , even in surface images (or below 5% of the low intensity images in the series presented here) (13).

Permeability Barrier Function—Transepidermal water loss was measured with an electrolytic water analyzer (MEECO, Warrington, PA). Individually tested sites were covered with Hilltop chambers (nominal volume 200 μl), which were reapplied following each individual measurement. For topical inhibitor applications, solutions of HEPES buffer (10 mM) at either pH 7.4 or 5.5, contained either amiloride (5 μM), HOE694 (7.5 μM), or buffer alone. The inhibitor-concentrations were chosen in the range of the published 50% inhibitory concentrations

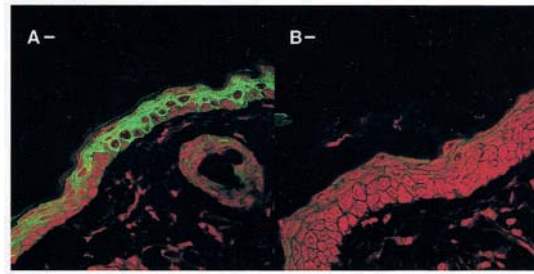


FIG. 1. Epidermal expression of NHE1. Sections were stained using a polyclonal anti-NHE1 antibody, detected with a FITC-labeled secondary antibody, counterstained with propidium iodide, and visualized on a Leica Confocal TCS SP microscope. The images represent the superposition of the green FITC label (NHE1) with the red propidium iodide label (DNA). Magnification bar represents 10 μm . *A*, NHE1 $+/+$ mice display increasing expression of NHE1 in more differentiated layers of the epidermis. *B*, to ensure the specificity of this staining pattern, we performed the same staining on NHE1 $-/-$ mouse skin. NHE1 staining was equal to background intensity under identical conditions.

(IC₅₀) for NHE1 inhibitory compounds in fibroblasts (22, 23).

The SC of hairless mice was removed from two sites by several sequential strippings with adhesive tape (Tesa, Beiersdorf, Germany), inducing an increase in transepidermal water loss levels above base line (from <0.2 to ~ 7 – 9 $\text{g}/\text{m}^2/\text{h}$). After stripping, inhibitors (conditions as above) were applied and transepidermal water loss was measured at 0, 2, 5, and 24 h. For studies in NHE1 knockout mice, homozygous ($-/-$) mice were compared with their wild-type ($+/+$) littermates, or age-matched wild-type animals of the same inbreeding generation. Flanks of these mice were shaved, and barrier homeostasis was studied between 48 and 96 h later. For tape-stripping of these animals, D-squame disks (Acadern, Menlo Park, CA) were used, as Tesa tape was too disruptive for application to shaved, hairy mouse skin.

Conventional surface pH measurements were performed using a flat glass surface electrode (Mettler-Toledo, Giessen, Germany) with a pH meter (Skin pH Meter PH 900; Courage & Khazaka, Cologne, Germany).

Ultrastructural Methods—Freshly obtained biopsies from mouse skin (inhibitor and buffer-treated hairless mice 5 h following tape-stripping; NHE1 $-/-$ and $+/+$ mice 8 h following tape-stripping, the time points that corresponded to the maximum delay in barrier recovery), were fixed directly in modified Karnovsky's fixative, postfixed with reduced osmium tetroxide (OsO₄), and then embedded in an Epon-epoxy mixture. For visualization of lipid-enriched, lamellar bilayer structures, some samples were postfixed with ruthenium tetroxide (RuO₄). Sections were cut on a Reichert Ultracut E microtome, counterstained with uranyl acetate and lead citrate, and viewed in a Zeiss 10 CR electron microscope, operated at 60 kV.

RESULTS

The Epidermal Localization of NHE1 Is Consistent with Its Putative Role in SC Acidification—We first assessed the localization of NHE1 in murine epidermis by immunohistochemistry. As seen in Fig. 1*A*, NHE1 is present in all epidermal cell layers. Its expression increases in the epidermal outer nucleated cell layers, especially in the apical surface of cells, and disappears in the enucleated cells above the SG-SC interface. Omission of the primary antibody eliminates virtually all epidermal staining (not shown). Immunostaining also is absent in NHE1 knockout ($-/-$) versus wild-type ($+/+$) epidermis (Fig. 1, *B* versus *A*), demonstrating the specificity of this labeling. These images demonstrate that NHE1 is expressed more abundantly in a suprabasal and apical pattern, consistent with a novel role in extracellular acidification of the SC.

Deletion of NHE1 Results in Reduced Acidification at the SG-SC Interface—Traditional skin surface pH measurements do not reveal detailed information about pH changes deep within the SC, or within specific microdomains (*e.g.* in the corneocyte interstices). Moreover, tape-stripping to measure pH in deeper levels of the SC, the only method available until

now, inevitably disturbs the tissue pH equilibrium. We therefore employed FLIM as a novel method to visualize pH in intact, unperturbed SC (13) and as a function of depth within the outer epidermis of NHE1 knockout mice (Fig. 2B) versus their wild-type littermates (Fig. 2A). FLIM measurements are dye concentration-independent, are not prone to photobleaching, and offer a look deep into intact tissue (19, 21). This method therefore reveals differential pH changes with great detail, here displayed as pH maps of the SC (13, 20). Because both surface pH and the slope of SC pH are important in epidermal barrier homeostasis (11), we measured pH at different levels of the SC. The increased spatial resolution of FLIM distinguishes differences in the pH of SC extracellular versus intracellular domains, as well as depth-dependent pH changes, conventionally referred to as the pH gradient (24). BCECF, the pH-sensitive indicator in these experiments, is used normally as an acetoxymethyl ester for intracellular measurements, because this uncharged molecule (but not the free acid BCECF) can permeate cell membranes (product information, Molecular Probes, Eugene, OR). Nevertheless, living cells do not exclude BCECF free acid completely (25). Using FLIM, we were able to measure the relative amounts of BCECF in the intracellular versus extracellular compartments, and found that BCECF free acid penetrates into cells (the ratio of intracellular to extracellular dye concentration in the SC is ~1:10), which we attribute to the nature of the SC, *i.e.* the enucleated corneocytes of this non-viable layer become more permeable and cannot exclude the dye effectively. Additionally, because of the increased sensitivity of FLIM, we also were able to detect BCECF in viable SG cells, albeit in much lower concentrations than seen in SC corneocytes.

In wild-type SC, FLIM reveals acidic (~ pH 6) and neutral (~ pH 6.8) areas (compare histograms in Fig. 2A), and the section-individual pH histograms show a change from predominantly acidic to a predominantly neutral pH from the upper to the lower SC (from outward to inward optical sections). Nevertheless, even at a depth that represents the SG-SC interface (6–8 μm), acidity is still present in extracellular microdomains, ensuring an optimal pH for enzymes such as β -Glc-Cer'ase and aSM'ase (6, 7), which are required for extracellular lipid processing. Because the outline of corneocytes can be seen clearly in the intensity images, intra- and extracellular values are identified through side-by-side comparison of intensity images (*left column*) and FLIM/pH maps (*center column*), which allows identification and localization of acidic microdomains to extracellular areas of the SC. Although the acidity of each microdomain is constant, the number of acidic microdomains increases in more superficial layers of the SC. The overall change in pH therefore lies in the number of acidic versus neutral areas (or in the number of acidic versus neutral pixels). In NHE1 $-/-$ mice, the acidic signal is almost completely absent from extracellular membrane domains (Fig. 2B) in the SC. In essence, the extracellular acidification is blunted in NHE1 $-/-$ SC (Fig. 2, A and B). Using three-dimensional histograms, we find that the acidic spike that corresponds to extracellular acidification starts in the lower SC and increases steadily in the NHE1 $+/+$ mice. In contrast, this acidic spike is missing completely in the NHE1 $-/-$ mice (Fig. 2C). The individual FLIM images (Fig. 2, A and B, *center column*) and the histograms derived from them (Fig. 2, A and B, *right column*) both demonstrate that the NHE1 is responsible for acidification of extracellular microdomains in SC.

To compare NHE1 wild-type and knockout animals further, three independent FLIM experiments per genotype were performed, and the pH of sections for the surface, and of SC/SG level were compared. The two-sided *t* test for these values confirms that the surface pH on the knockout and wild-type

mice are significantly different (Table I). However, the NHE1 $-/-$ pH measurements do not differ when surface and SC/SG interface pH are compared, consistent with an inability to acidify the SC in NHE1 $-/-$ skin to normal levels.

When FLIM was compared with standard flat electrode measurements, we found that many of the changes seen with FLIM were not distinguishable using the flat electrode, which suffers both from lower sensitivity and lower spatial resolution. For example, skin surface pH of NHE1 $-/-$ animals as measured with the flat electrode was only slightly but significantly elevated in comparison to their NHE1 $+/+$ littermates (pH 6.01 versus pH 5.75, $p = 0.02$, $n = 13$ and 15, respectively; compare with Fig. 2). The difference in absolute pH values between FLIM and flat surface pH electrode may also demonstrate the introduction of another artifact, the water necessary to wet the glass electrode, which further reduces the sensitivity of the glass electrode. Because the abnormalities seen with FLIM correlate with functional abnormalities in lipid processing and epidermal barrier repair (see below), we conclude that the flat electrode is not adequate to study some physiologically important changes in SC pH.

In summary, comparing epidermal structure via dye distribution with pH distribution maps, acidic pH localizes predominantly to extracellular domains of the SC, and acidity is almost completely absent from extracellular domains of NHE1 $-/-$ SC.

Permeability Barrier Homeostasis Is Abnormal in Transgenic NHE1 Knockout Mice—To determine the importance of epidermal acidification through NHE1, we next examined its function in epidermal barrier homeostasis of NHE1 $-/-$ mice. Although the $-/-$ animals were somewhat smaller than either their wild-type or heterozygous littermates at the time of weaning and displayed an ataxic gait as part of the reported epilepsy (14, 26), the skin of knockout animals appeared clinically and histologically normal. Transepidermal water loss as a measure of permeability barrier function in $-/-$ mice did not differ from $+/+$ littermates at base line (data not shown), demonstrating that the smaller size of affected animals did not cause a non-specific epidermal barrier defect. However, differences in barrier homeostasis between knockout and wild-type animals became apparent after barrier disruption by sequential removal of the outermost SC layers by gentle tape-stripping (Fig. 3a). NHE1 $-/-$ animals had slower barrier recovery, with significant differences at both 5 and 8 h after tape-stripping ($-/-$ animals versus $+/+$ littermates, $p < 0.005$, two-tailed *t* test). Barrier recovery kinetics of NHE1 $-/-$ mice was similar to those of normal, hairless mice treated with the NHE1 inhibitor HOE694 (results below; *c.f.* Fig. 4a). These results demonstrate that the presence or absence of the NHE1 antiporter has important functional consequences for normal epidermal permeability barrier homeostasis.

NHE1 Inhibition Delays Epidermal Permeability Barrier Recovery in a pH-dependent Manner—As a second model to confirm whether NHE1-mediated SC acidification is linked to barrier function, we inhibited the NHE1 pharmacologically. We focused on the kinetics of barrier recovery, again assessed as changes in transepidermal water loss rates, after acute barrier perturbations by tape-stripping, followed by exposure to buffers of different pHs with or without added inhibitors. We compared the effects of amiloride as the prototypical NHE inhibitor (27, 28) with the highly specific NHE1 inhibitor HOE694 (29) at various doses on permeability barrier homeostasis. When amiloride was applied after tape-stripping in a concentration range, based upon its reported IC_{50} in fibroblasts (*i.e.* 5 μM), a significant delay in barrier recovery occurred at 2 and 5 h, with normalization of recovery by 24 h. Although in cell culture and

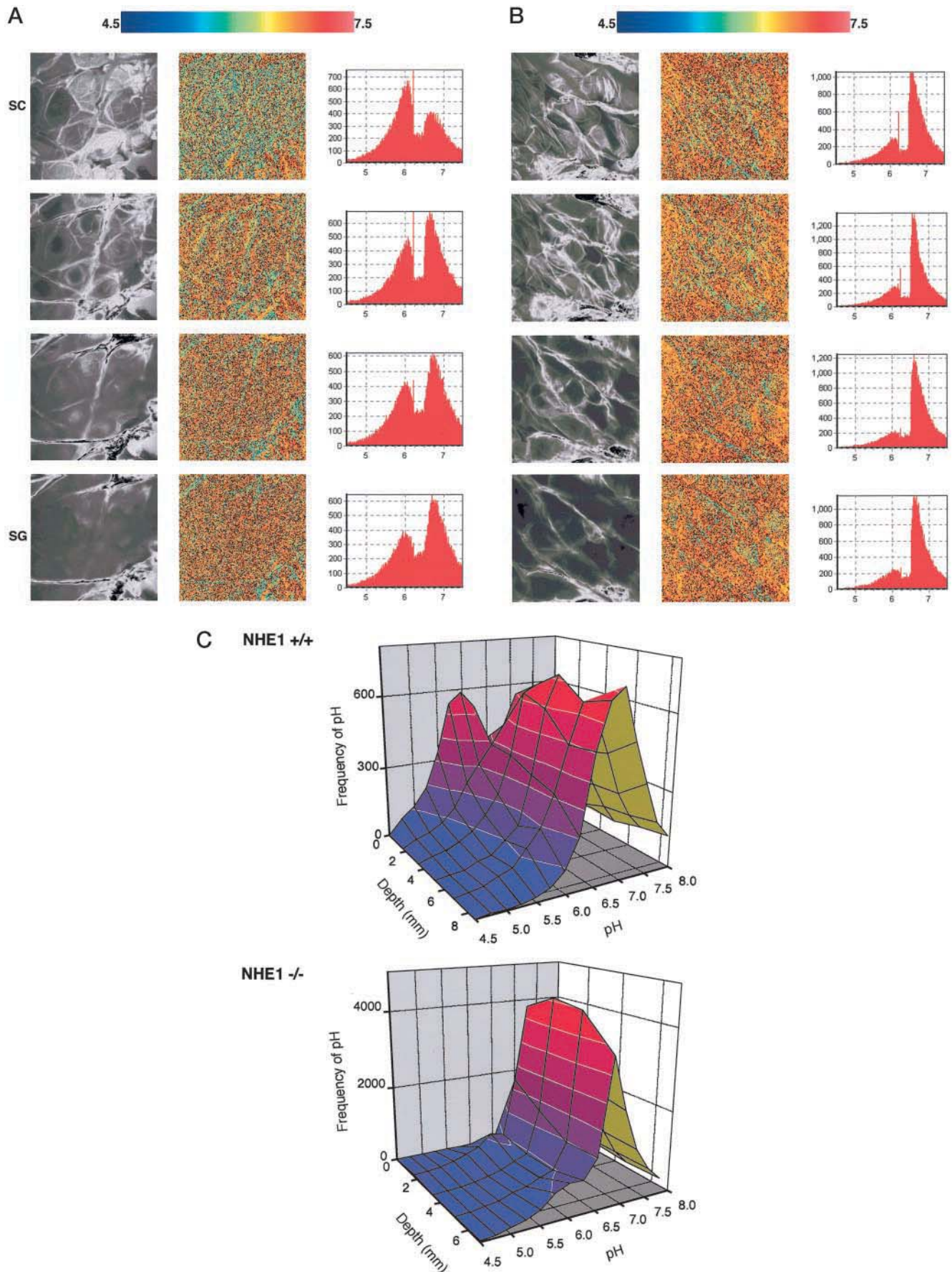


FIG. 2. Fluorescence lifetime imaging of NHE1 wild-type and knockout epidermis. Skin of hairy, shaved mice was incubated with BCECF, then prepared and visualized as described under “Experimental Procedures.” A, fluorescence lifetime Images of NHE1 +/+ mice. A series of four consecutive, non-overlapping images/optical sections, *en face* view extending from the SC surface (0 μ m) to the SC-SG interface

TABLE I
Comparison of SC pH in NHE1 wild type and knockout

To compare pH changes between NHE1 wild-type and knockout animals statistically, three independent FLIM experiments per genotype were performed, and the pH of sections for the surface, and of SC/SG level were compared. The two-sided *t* test for these values confirms that the surface pH on the knockout and wild-type mice are significantly different. However, the NHE1 $-/-$ pH measurements do not differ when surface and SC/SG interface pH are compared, consistent with an inability to acidify the SC in NHE1 $-/-$ skin to normal levels.

NHE1	pH	Deviation	S.E.	<i>t</i> test	
				SC vs. SG	Wild-type vs. knockout
Wild-type (<i>n</i> = 3)	SC	6.18	0.041	0.02	SC: 0.01
	SG	6.34	0.052		
Knockout (<i>n</i> = 3)	SC	6.38	0.047	0.64	SG: 0.27
	SG	6.40	0.040		

in short term measurements of intracellular pH, 1 μ M amiloride is fully inhibitory (1), the extent of barrier recovery at 24 h may be attributable to the lower specificity for NHE1 (see also the ultrastructural findings below). When HOE694 was applied to acutely disrupted skin sites at 1.5 μ M, a significant delay in barrier recovery rates also occurred, which was sustained out to 24 h. A 10-fold increase in HOE694 concentration (to 15 μ M) produced a more marked functional abnormality, with only 50% normalization of barrier function at 24 h. The lack of an additional increase in absolute transepidermal water loss levels with the highest concentration tested (*i.e.* 15 μ M) makes a toxic effect highly unlikely (signs of toxicity were also absent by ultrastructural examination; Fig. 4b). Nevertheless, further experiments, described below (Fig. 4a), utilized HOE694 at an intermediate concentration (*i.e.* 7.5 μ M). Finally, to establish that the barrier defect is linked to an acidification abnormality, we assessed whether co-applications of an acidic buffer with the inhibitors would normalize barrier recovery. Co-applications of an acidic buffer with HOE694 overrode the effects of the inhibitor alone (Fig. 4a), demonstrating that the abnormalities in permeability barrier homeostasis are caused by NHE1-inhibitor-induced alterations in SC acidification.

Blockade or Deletion of NHE1 Results in Altered Extracellular Lipid Processing—The structural basis for the knockout and inhibitor-induced delays in barrier recovery was assessed by electron microscopy. Because previous studies found that neutralization of the SC pH gradient impaired epidermal barrier recovery by preventing the processing of secreted lipids (3), whereas the lamellar body delivery system remained unaltered (30), we surveyed lamellar body formation and secretion, as well as the post-secretory, extracellular processing of lipids in NHE1 $-/-$, HOE694-, and amiloride-treated animals.

Electron micrographs of NHE1 $-/-$ epidermis revealed a defect in lamellar membrane maturation at the time of maximum delay in epidermal barrier recovery, *i.e.* 8 h following barrier disruption (Fig. 3b, panel D; compare with $+/+$, panel C), but not under basal conditions (Fig. 3b, panels A and B). Moreover, the morphology of NHE1 $-/-$ SC resembled that in HOE694-treated mice at comparable time points after epidermal barrier disruption (*c.f.* Fig. 4b, panel B). In numerous areas of the lower SC, lipid processing was delayed, assessed both as a persistence of newly secreted lipids, and the presence of incompletely processed (“immature”) lamellar membrane structures several layers above the SG-SC interface.

Our earlier study demonstrated that exposure to a neutral pH buffer delayed epidermal barrier recovery through an inhi-

bition of extracellular processing, rather than through lamellar body formation/secretion (3). Likewise, micrographs of HOE694-treated epidermis revealed undisturbed lamellar body formation and secretion, as well as an absence of any signs of cytotoxicity (Fig. 4b, panels B and C), comparable to both skin exposed to pH 5.5 (data not shown) and wild-type epidermis (Fig. 3b, panels A and C). However, as with exposure to a neutral pH buffer (3), HOE694 applications provoked the appearance of abnormal lamellar membranes, observed with ruthenium tetroxide after fixation as the persistence of incompletely processed (immature) extracellular lamellar bilayers several layers above the SG-SC interface (Fig. 4b, panel B). In contrast, controls from both inhibitor and transgenic experiments demonstrated completely processed bilayers, already present at the SG-SC interface and within the first layer of the SC (Fig. 4b, panel A; Fig. 3b, panels A and C). Moreover, when HOE694 was co-applied in an acidic buffer, lamellar membrane maturation was normal. In contrast to HOE694-treated skin, however, amiloride treatment leads not only to the expected abnormality in lipid processing, but also to premature lipid secretion, an effect attributable to blockade of the ENaC channel (31), which was absent in HOE694 treatment (Fig. 4b, panel C; amiloride images not shown).

Pharmacologic (HOE694)-induced NHE1 blockade results in morphologic effects that an acidic solution can override. These delays are consistent with and equivalent to epidermal barrier recovery of NHE1 $-/-$ mice, strongly suggesting that NHE1-mediated acidification influences epidermal barrier homeostasis primarily through its action on pH-sensitive extracellular lipid processing events.

DISCUSSION

Role of the NHE1—We show here that NHE1 not only has a novel function in acidifying the extracellular lipid domain of the SC, but also that the SC acidity generated by this mechanism influences cutaneous permeability barrier homeostasis and lipid processing, as evidenced by results comparing normal to HOE694-treated and NHE1 $+/+$ and $-/-$ mice. Whereas the NHE1 modulates SC pH, it localizes primarily to the last nucleated layer of the epidermis, the SG, and not to the SC where acidification and barrier function occurs/resides. Moreover, SC pH seemingly becomes progressively more acidic in the outer SC, furthest from the location of the NHE1, rather than in the regions contiguous to the active antiporter. This apparent paradox is resolved when the topography of SC pH is examined using a more sophisticated method; *i.e.* fluorescence lifetime

(approximately 6 μ m into the epidermis) of untreated mouse skin. Fluorescence intensity images (*left*), compared with fluorescence lifetime, which was converted to pH maps (*middle column*), and a histogram of this pH distribution (*right*); pH color scale at *top*. B, FLIM images for NHE1 $-/-$ mice, presented in the same fashion as in A. Note the lesser variation of pH values in the pH maps, and unchanging pH profile in the histograms. C, pH changes as a function of tissue depth within intact epidermis of both NHE1 $+/+$ (A) and $-/-$ mice (B). Three-dimensional combination of the individual pH histograms shown in A and B (*right columns*). The decreasing acidity over the first 0–6 μ m depicts the SC pH gradient, and remaining acidity in deeper SC layers of NHE1 $+/+$ mice reveals the previously unknown acidic microdomains. In contrast, the almost complete absence of acidity throughout the SC of NHE1 $-/-$ mice reveals the importance of NHE1 for SC acidification.

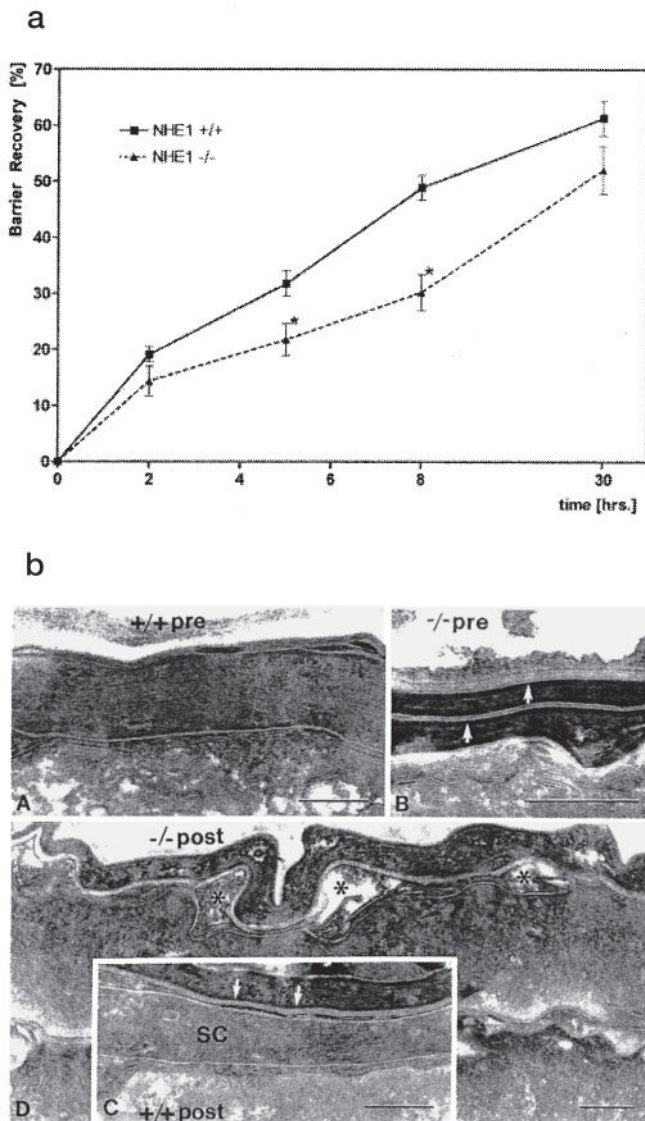


FIG. 3. *a*, barrier recovery of NHE1 $-/-$ mice compared with their $+/+$ littermates. Paired mice were shaved and tape-stripped following an interval of at least 48 h. Barrier recovery was monitored for 30 h. Graphed values represent means of ≥ 28 individual measurements; *, p values are < 0.05 , two-tailed t test. *b*, NHE1 $-/-$ ultrastructure. Electron micrographs of NHE1 $-/-$ mouse skin, compared with wild-type (RuO₄ postfixation; magnification bars represent 0.25 μ m). Before tape-stripping (*pre*), wild-type skin (*A*) displays regular epidermal architecture, lipid secretion, and processing (arrowheads; RuO₄ postfixation). *B*, the $-/-$ mice also show regular SC structure (arrowheads) and extracellular lipid secretion proceeds regularly. 8 h after tape-stripping (*post*), the wild-type (*C*) shows regularly processed bilayers within SC extracellular domains, whereas in the knockout (*D*) abnormal lipid processing, lacunae of unprocessed lipid (*), is visible.

imaging microscopy (FLIM). Previous studies demonstrate that initial lipid processing normally occurs in extracellular domains (3), and that it is this initial lipid processing step, at the SG-SC interface and in the lower SC, that is disturbed in: 1) neutral buffer-exposed skin, 2) NHE1 $-/-$ mice, and 3) normal mice treated with the specific NHE1 inhibitor, HOE694. This view is supported by insights from other knockout models/diseases, which also reveal the SG-SC interface to be an area of intense enzymatic lipid processing activity (5–7, 32). Here we show with FLIM that this compartment is already acidified in normal skin, contrary to the conventional view of the pH gradient obtained with flat electrodes, which would predict this compartment to be neutral. This finding is consistent with the

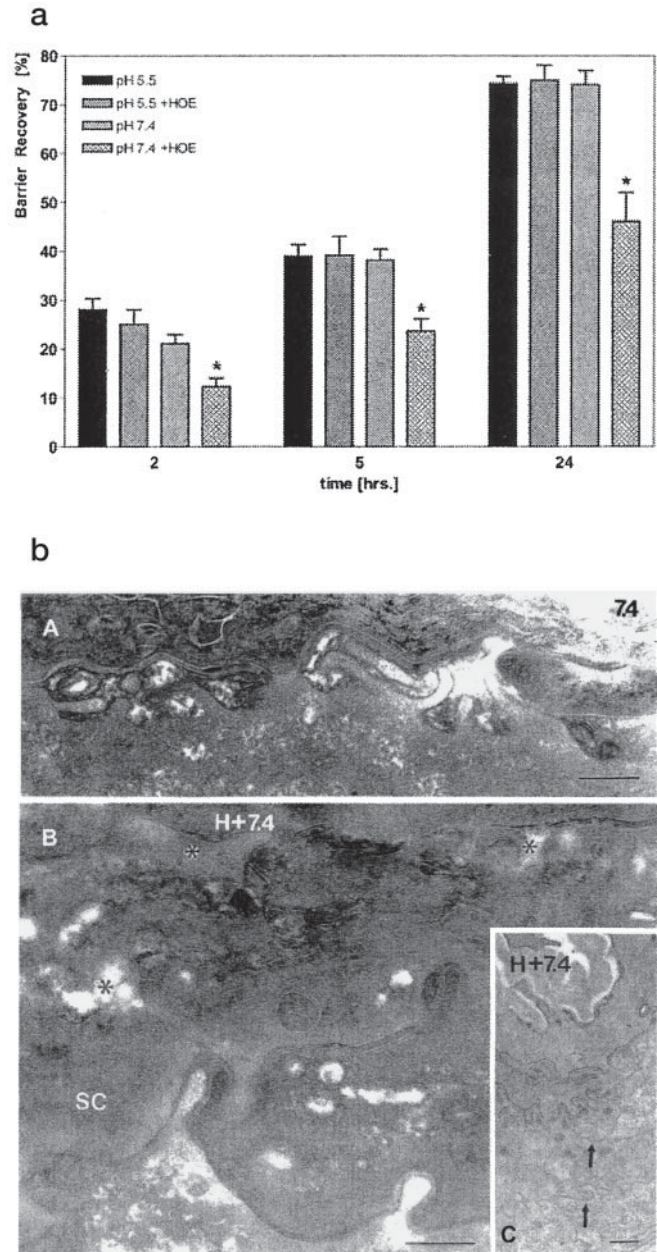


FIG. 4. *a*, effect of pH and NHE1 inhibition on barrier recovery. Hairless mice were tape-stripped to transepidermal water loss of 7–9 g/m²/h and Hilltop chambers with or without HOE694 (7.5 μ M) in pH 7.4 or 5.5 HEPES buffer (10 mM) were applied. Control areas were covered with Hilltop chambers containing HEPES buffer (10 mM) of pH 5.5 and 7.4, respectively. Transepidermal water loss was measured at 0, 2, 5, and 24 h following tape-stripping, and the same Hilltop chambers were reapplied immediately following measurements. Graphed values represent percentage of recovery from the defect induced by tape-stripping. Depicted are means of ≥ 14 individual measurements for HOE694; *, p values are < 0.05 , two-tailed t test. *b*, NHE1-inhibitor/pH-dependent ultrastructure. Electron micrographs of hairless mouse skin biopsies taken at 5 h following tape-stripping, incubated with HEPES buffer of pH 7.4. (Magnification bars in *A* and *B* represent 0.25 μ m; bar represents 0.5 μ m in *C*.) *A*, incubation with HEPES buffer of pH 7.4, no changes in lipid secretion and extracellular processing (RuO₄ postfixation); *B*, addition of HOE694 (*H*), intercellular lacunae (*) of unprocessed lipid persist within the SC (RuO₄ postfixation); *C*, lipid secretion proceeds normally (arrowheads; OsO₄ postfixation).

known sites of lipid processing of β -Glc-Cer'ase and aSM'ase (5–7).

Although intracellular pH has been linked to diverse cellular functions in various tissues, including cell proliferation, trans-

formation, and differentiation (1, 33, 34), extracellular acidification also occurs in a regulated manner. The NHE family of Na^+/H^+ exchangers is ubiquitous, and their role in acid-base balance is best understood in kidney (33), where concentration-driven influx of Na^+ provides the driving force for the NHE-mediated extrusion of H^+ into the extracellular domain. NHE1 and NHE3 are responsible for intracellular pH regulation, but also H^+ secretion/ HCO_3^- reabsorption along the proximal nephron (33, 35). In osteoclasts, as in SC, NHE1 is responsible for H^+ secretion, which, similar to SC, occurs in localized microdomains (reviewed in Ref. 36). Thus, the SC may have adapted the ubiquitous ability of the NHE1 to secrete H^+ to a specialized function, *i.e.* acidification of microdomains in the lower SC. In recent years, NHE1 has been shown to assume unexpected functions, in cell adhesion and spreading through effects on structural filaments (37). To this list, we now add the function of regulating epidermal barrier homeostasis through control of SC pH and lipid processing.

Although the NHE1 is present in highest quantities in the terminal nucleated cell layers of the epidermis (*i.e.* the SG), several lines of evidence argue that impairment of lipid processing, not impairment of keratinocyte differentiation, at the interface between SG and SC is the primary defect when the NHE1 is disabled. First, we observed normal appearing keratinocyte differentiation, and normal epidermal and keratinocyte cellular morphology in HOE694-treated and NHE1 $-/-$ mice, suggesting that cellular function(s) are mostly normal. Second, epidermal barrier repair and lipid processing were impeded within 2 h of pharmacologic inhibitor treatment, an interval during which effects on cell growth and differentiation are minimal. Finally, following tape-stripping, lamellar body formation and lipid secretion, but not lipid processing, appear normal in NHE1 $-/-$ mice. The potential indirect effects of altered intracellular acidity on these extracellular events remain to be determined.

Generation and Measurement of the SC pH Gradient—The acid mantle of the SC is postulated to regulate several key epidermal functions, including epidermal barrier homeostasis (3, 38, 39), desquamation (11), and antimicrobial capacity (40, 41). Formation of a competent epidermal barrier requires two processes: synthesis and secretion of lipid from SG cells into the lower SC interstices, followed by processing of the secreted lipid into functionally competent lamellar membranes. Although secretion is controlled by extracellular Ca^{2+} and K^+ concentrations (30), processing is regulated by fluctuations in extracellular pH (3). The acidic SC appears to control lipid processing and epidermal barrier homeostasis through two or more pH-dependent, lipid hydrolases (β -Glc-Cer'ase, aSM'ase), that are essential for the extracellular processing of SC lipid precursors. These hydrolases, which generate the complete family of seven epidermis-unique ceramides from glucosylceramides and sphingomyelin (42), become inactive when SC is exposed to a neutral pH (3), consistent with their known acidic pH optimum (5–7).

Traditionally, pH has been assessed in the mammalian SC using a flat pH electrode, accessing progressively lower layers of the SC by removal of sequential SC layers with tape-stripping. This flat electrode method, introduced in 1939 (43), is not only inherently disruptive, but it is an “averaging method” that can only assess mean pH across a wide area. Such a method can neither distinguish between intracellular and extracellular pH, nor identify microdomains of greater or lesser pH in close proximity within the SC. Using FLIM to measure and simultaneously visualize pH distribution, we identified previously unknown, acidic membrane compartments, “microdomains,” at the SG-SC interface, and in the lower SC interstices, revealing

significant complexities in the SC pH gradient. Unlike tape-stripping, FLIM does not disrupt the SC to measure pH in the lower SC layers. Moreover, FLIM measurements eliminate other potential artifacts usually inherent to a fluorescent dye approach, as they do not result in photobleaching and are independent of pH-sensing dye concentration (especially important as the barrier properties of skin create a dye gradient (Ref. 44)). Still, the physical dimensions of the two-photon focus, or the point-spread function of the microscopic system, limit the resolution and determination of intra- versus extracellular compartments within the SC. Nevertheless, the extracellular domains as present in the *en-face* view that this system generates should be rather homogeneous, based on the columnar stacking of corneocytes (45–48), whereas the horizontal inter-corneocyte spaces are small compared with the corneocyte volume; the error based on the assignment of specific compartments should therefore be small.

FLIM therefore provides novel insights into the generation and spatial distribution of acidic microdomains, which may alter the current view of potential contributors to SC acidity. Previously, a number of mechanisms have been proposed as sources for the acidic surface of skin. In general, these sources can be viewed as catabolic processes within the SC, providing acidic end products. For example, the breakdown of proteins (and the generation of the organic acid cUCA from filaggrin (Ref. 12)) or lipids (phospholipid hydrolysis to free fatty acids (Ref. 10)), either intrinsically through specific enzymes, or as byproducts of microbial metabolism (8), has received most attention. Additionally, through skin appendages, acidic material may be deposited onto the SC surface, *e.g.* lactic acid and lactate from sweat (9) and sebum-derived free fatty acids (49).

cUCA generation in SC as a mechanism for acidification, while providing a compelling mathematical concept (12), to date has not been thoroughly tested. Further, it cannot explain acidification at the SG-SC interface but rather complies with the conventional view of an inner-to-outer SC pH gradient. Additionally, such a mechanism would predict a more acidic pH within the corneocytes themselves, where cUCA is generated from abundant filaggrin. Similarly, how free fatty acids as lipophilic compounds can contribute to acidity in a generally dry environment is not fully understood. However, several studies indicate that formation of the ordered extracellular lipid bilayer structures, which include free fatty acids, requires an acidic pH rather than creating it (49–51). Further, the phospholipases known to date to be present in SC and responsible for cleavage of phospholipids (52) exhibit general characteristics that may indicate a dependence on neutral pH, and requiring millimolar calcium concentrations (reviewed in Ref. 53). Therefore, recent results with pharmacologic soluble phospholipase A_2 inhibition demonstrating changes in surface pH (10), but only a delayed effect on SC lipid composition (54), should be viewed with caution, especially in light of the unknown specificity of the soluble phospholipase A_2 inhibitors used (55). Microbial metabolism, sweat, and sebum, although they may be significant contributors to the very surface of SC, do not readily explain acidified compartments in deeper SC layers. Finally, these processes vary greatly as a result of seasonal changes, body type, and age, and may therefore not be able to provide sufficient acidity at all times and in an evenly distributed fashion over the whole integument.

In contrast, our experiments provide evidence for an intrinsic, regulated pathway that can supply protons directly to the SC compartment, where enzymatic activity requires acidity, and where proper epidermal function is dependent on it. Furthermore, this effect appears to be specific for and to the SC, as pH in the SG layer does not change in NHE1 $-/-$ mice, where

SC acidity is absent. Nevertheless, any or all of the mechanisms discussed above could contribute to additional acidification following the initial NHE1-mediated microdomain acidification at the SG-SC junction.

In summary, the experiments described above demonstrate that NHE1 inactivation alone is sufficient to impede SC acidification, and specifically to alter pH at a critical domain, *i.e.* the SG-SC interface and lower SC. We speculate, therefore, that the NHE1 provides the initial step in establishing the SC acidity required for lipid processing that leads to a functional permeability barrier in normal epidermis, whereas other pathways may contribute acidic components in more superficial SC layers.

REFERENCES

1. Mauro, T., Dixon, D. B., Hanley, K., Isseroff, R. R., and Pappone, P. A. (1995) *J. Invest. Dermatol.* **105**, 203–208
2. Sarangarajan, R., Shumaker, H., Soleimani, M., Le Poole, C., and Boissy, R. E. (2001) *Biochim. Biophys. Acta* **1511**, 181–192
3. Mauro, T., Holleran, W. M., Grayson, S., Gao, W. N., Man, M. Q., Kriehuber, E., Behne, M., Feingold, K. R., and Elias, P. M. (1998) *Arch. Dermatol. Res.* **290**, 215–222
4. Holleran, W. M., Takagi, Y., Imokawa, G., Jackson, S., Lee, J. M., and Elias, P. M. (1992) *J. Lipid Res.* **33**, 1201–1209
5. Takagi, Y., Kriehuber, E., Imokawa, G., Elias, P. M., and Holleran, W. M. (1999) *J. Lipid Res.* **40**, 861–869
6. Schmuth, M., Man, M. Q., Weber, F., Gao, W., Feingold, K. R., Fritsch, P., Elias, P. M., and Holleran, W. M. (2000) *J. Invest. Dermatol.* **115**, 459–466
7. Jensen, J. M., Schutze, S., Forl, M., Kronke, M., and Proksch, E. (1999) *J. Clin. Invest.* **104**, 1761–1770
8. Korting, H. C., Kober, M., Mueller, M., and Braun-Falco, O. (1987) *Acta Derm. Venereol.* **67**, 41–47
9. Patterson, M. J., Galloway, S. D., and Nimmo, M. A. (2000) *Exp. Physiol.* **85**, 869–875
10. Fluhr, J. W., Kao, J., Jain, M., Ahn, S. K., Feingold, K. R., and Elias, P. M. (2001) *J. Invest. Dermatol.* **117**, 44–51
11. Ohman, H., and Vahlquist, A. (1998) *J. Invest. Dermatol.* **111**, 674–677
12. Krien, P. M., and Kermici, M. (2000) *J. Invest. Dermatol.* **115**, 414–420
13. Hanson, K. M., Behne, M. J., Barry, N. P., Mauro, T. M., Gratton, E., and Clegg, R. M. (2002) *Biophys. J.* **83**, 1682–1690
14. Bell, S. M., Schreiner, C. M., Schultheis, P. J., Miller, M. L., Evans, R. L., Vorhees, C. V., Shull, G. E., and Scott, W. J. (1999) *Am. J. Physiol.* **276**, C788–C795
15. Man, M. Q., Feingold, K. R., and Elias, P. M. (1993) *Arch. Dermatol.* **129**, 728–738
16. Menon, G. K., and Elias, P. M. (1997) *Skin Pharmacol.* **10**, 235–246
17. Komuves, L. G., Hanley, K., Man, M. Q., Elias, P. M., Williams, M. L., and Feingold, K. R. (2000) *J. Invest. Dermatol.* **115**, 361–367
18. Menon, G. K., Feingold, K. R., Mao-Qiang, M., Schaub, M., and Elias, P. M. (1992) *J. Invest. Dermatol.* **98**, 209–219
19. Masters, B. R., So, P. T., and Gratton, E. (1997) *Biophys. J.* **72**, 2405–2412
20. Szmajkowski, H., and Lakowicz, J. R. (1993) *Anal. Chem.* **65**, 1668–1674
21. Tadrous, P. J. (2000) *J. Pathol.* **191**, 229–234
22. Noel, J., and Pouyssegur, J. (1995) *Am. J. Physiol.* **268**, C283–C296
23. Counillon, L., Scholz, W., Lang, H. J., and Pouyssegur, J. (1993) *Mol. Pharmacol.* **44**, 1041–1045
24. Ohman, H., and Vahlquist, A. (1994) *Acta Derm. Venereol.* **74**, 375–379
25. Sit, K. H., Bay, B. H., and Wong, K. P. (1993) *Anat. Rec.* **235**, 183–190
26. Bonnet, U., Bingmann, D., and Wiemann, M. (2000) *Eur. Neuropsychopharmacol.* **10**, 97–103
27. Vigne, P., Frelin, C., Cragoe, E. J., Jr., and Lazdunski, M. (1984) *Mol. Pharmacol.* **25**, 131–136
28. Frelin, C., Vigne, P., Barbry, P., and Lazdunski, M. (1987) *Kidney Int.* **32**, 785–793
29. Loh, S. H., Sun, B., and Vaughan-Jones, R. D. (1996) *Br. J. Pharmacol.* **118**, 1905–1912
30. Lee, S. H., Elias, P. M., Feingold, K. R., and Mauro, T. (1994) *J. Invest. Dermatol.* **102**, 976–979
31. Mauro, T., Guitard, M., Behne, M., Oda, Y., Crumrine, D., Komuves, L., Rassner, U., Elias, P. M., and Hummler, E. (2002) *J. Invest. Dermatol.* **118**, 589–594
32. Holleran, W. M., Takagi, Y., Menon, G. K., Legler, G., Feingold, K. R., and Elias, P. M. (1993) *J. Clin. Invest.* **91**, 1656–1664
33. Capasso, G., Saviano, C., Rizzo, M., Pica, A., Capodicasa, D., Mascolo, N., and De Santo, N. G. (1997) *Miner. Electrolyte Metab.* **23**, 243–248
34. Reshkin, S. J., Bellizzi, A., Caldeira, S., Albarani, V., Malanchi, I., Poignee, M., Alunni-Fabbroni, M., Casavola, V., and Tommasino, M. (2000) *FASEB J.* **14**, 2185–2197
35. Pannabecker, T. L., Brokl, O. H., Kim, Y. K., Abbott, D. E., and Dantzer, W. H. (2002) *Pflugers Arch.* **443**, 446–457
36. Rousselle, A. V., and Heymann, D. (2002) *Bone* **30**, 533–540
37. Tominaga, T., and Barber, D. L. (1998) *Mol. Biol. Cell* **9**, 2287–2303
38. Thune, P., Nilsen, T., Hanstad, I. K., Gustavsen, T., and Lovig Dahl, H. (1988) *Acta Derm. Venereol.* **68**, 277–283
39. Berg, R. W., Milligan, M. C., and Sarbaugh, F. C. (1994) *Pediatr. Dermatol.* **11**, 18–20
40. Aly, R., Shirley, C., Cunico, B., and Maibach, H. I. (1978) *J. Invest. Dermatol.* **71**, 378–381
41. Korting, H. C., Hubner, K., Greiner, K., Hamm, G., and Braun-Falco, O. (1990) *Acta Derm. Venereol.* **70**, 429–431
42. Uchida, Y., Behne, M., Quiec, D., Elias, P. M., and Holleran, W. M. (2001) *J. Invest. Dermatol.* **117**, 1307–1313
43. Blank, I. H. (1939) *J. Invest. Dermatol.* **2**, 67
44. Turner, N. G., Cullander, C., and Guy, R. H. (1998) *J. Invest. Dermatol. Symp. Proc.* **3**, 110–113
45. Wepf, R., Richter, T., Koenig, K., Dunkelmann, K., Sattler, M., Biel, S., Hintze, U., and Wittern, K. P. (2002) *J. Invest. Dermatol.* **119**, 250 (Abstr. 256)
46. Mackenzie, I. C., Zimmerman, K., and Peterson, L. (1981) *J. Invest. Dermatol.* **76**, 459–461
47. Mackenzie, J. C. (1969) *Nature* **222**, 881–882
48. Christophers, E. (1971) *J. Invest. Dermatol.* **56**, 165–169
49. Lieckfeldt, R., Villalain, J., Gomez-Fernandez, J. C., and Lee, G. (1995) *Pharm. Res. (N. Y.)* **12**, 1614–1617
50. Bouwstra, J. A., Gooris, G. S., Dubbelaar, F. E., Weerheim, A. M., and Ponc, M. (1998) *J. Invest. Dermatol. Symp. Proc.* **3**, 69–74
51. Bouwstra, J. A., Gooris, G. S., Dubbelaar, F. E., and Ponc, M. (2000) *Cell. Mol. Biol.* **46**, 979–992
52. Schadow, A., Scholz-Pedretti, K., Lambeau, G., Gelb, M. H., Furstenberger, G., Pfeilschifter, J., and Kaszkin, M. (2001) *J. Invest. Dermatol.* **116**, 31–39
53. Six, D. A., and Dennis, E. A. (2000) *Biochim. Biophys. Acta* **1488**, 1–19
54. Mao-Qiang, M., Jain, M., Feingold, K. R., and Elias, P. M. (1996) *J. Invest. Dermatol.* **106**, 57–63
55. Ogata, Y., Sakurai, T., Nakao, S., Kuboyama, N., Moriwaki, K., Furuyama, S., and Sugiyama, H. (2002) *Comp. Biochem. Physiol. C Toxicol. Pharmacol.* **131**, 315–322